Spatio-Spectral Multichannel Reconstruction from few Low-Resolution Multispectral Data

Mohamed Elamine HADJ-YOUCEF [1,2]
François ORIEUX [1,2] Aurélia FRAYSSE [1] Alain ABERGEL [2]

[1]Laboratoire des Signaux et Systèmes (L2S)
CNRS, CentraleSupélec, Université Paris-Saclay, France

[2]Institut d'Astrophysique Spatiale (IAS)
CNRS, Univ. Paris-Sud, Université Paris-Saclay, France

September 06, 2018

Context

The James Webb Space Telescope (JWST) :

Organization	**NASA (ESA & CSA)**
Expected Launch	**March 2021**
Primary Mirror	$\mathbf{25}$ m^2 ($>3\times$ Hubble)
	$\mathbf{18}$ hexagonal segments
Wavelength Range	$\mathbf{5} - \mathbf{28}$ μm (factor of $\mathbf{5}$)

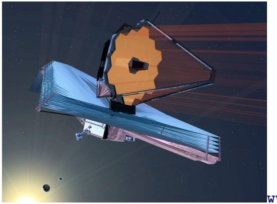

www.jwst.nasa.gov

Main objectives of the JWST mission :

- Studying the formation and evolution of galaxies
- Understanding formation of stars and exoplanetary system

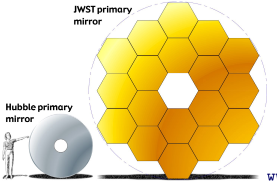

www.jwst.nasa.gov/mirrors

Instruments on board the JWST

Instrument and Data resolution :

Data	Spatial resolution	Spectral resolution
Imager	✓	✗
Spectrometer	✗	✓

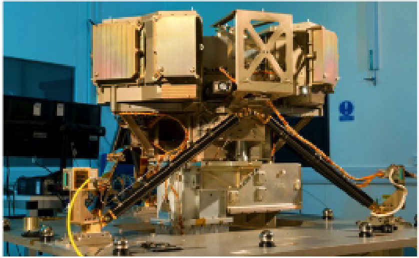

Mid-IR Instrument (MIRI) Imager [Bouchet]

Characteristics :

- **9** spectral bands $[5 - 28\ \mu\mathrm{m}]$
- $\lambda/\triangle\lambda \sim$ **5**
- Field of View $74'' \times 113''$
- **2D** detector matrix

Outline

1. Introduction
   - Objective and Problems
   - Related Works
2. Proposed Methodology
   - 1) Instrument Model
   - 2) Forward model
   - 3) Reconstruction
3. Results
4. Conclusion and Perspectives

Inverse Problem Application

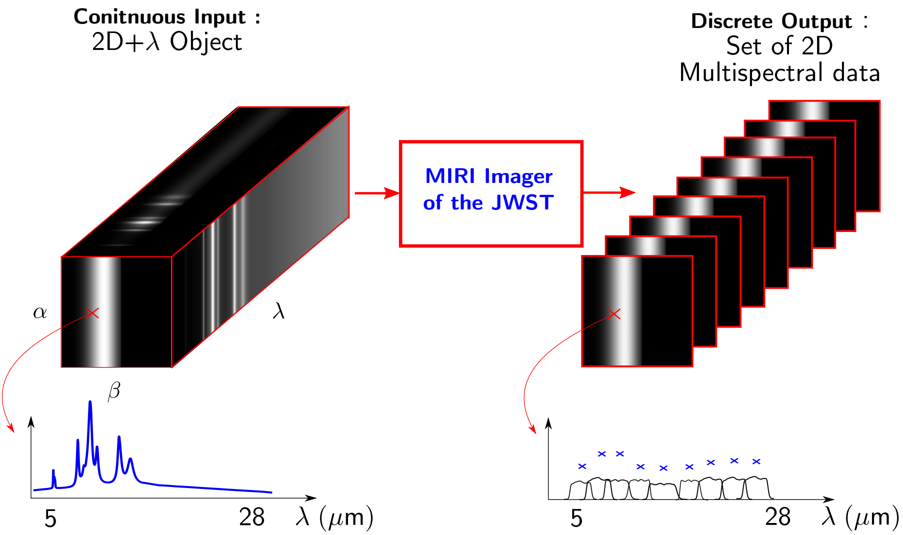

Objective and Problems

Main Objective

- Reconstruction of a high-resolution spatio-spectral object from a small number of degraded multispectral data

Problems

- Dependence of the optical system response (PSF) on the wavelength $\rightarrow$ Varying blur of the multispectral data
- Integration over broad windows $\rightarrow$ Low spectral resolution of the multispectral data
- Under-determined problem $\rightarrow$ Small number of multispectral data (e.g. only nine for the MIRI Imager)

Related Works

- Methods using stationary/non-stationary PSF :
  - Measured PSF [Guillard], Broadband PSF [Geis & Lutz 2010], PSF linear interpolation [Soulez], PSF approximation [Villeneuve & Carfantan 2014]

  $\rightarrow$ Neglect the spectral variation of the PSF = inaccurate response
- Processing of the data : Separately band per band [Aniano]

  $\rightarrow$ Neglect the cross-correlation between the spectral channel
- Our work in [Hadj-Youcef] (*26-th EUSIPCO*)

  $\rightarrow$ Limitation in the reconstruction of the spectral distribution

Propositions :

- Modeling the instrument response : spectral integration and variation of the optical response
- Joint processing of all the multispectral data

Modeling of the Instrument Response

Block diagram of the instrument model :

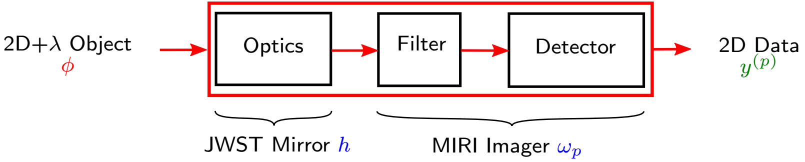

Spectral Variations of the PSF : h

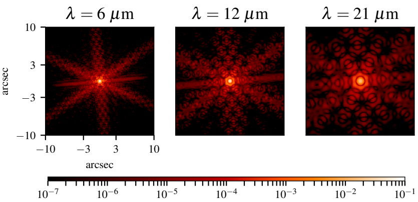

PSF using *WebbPSF* [Perrin]

Spectral Responses : ω_p

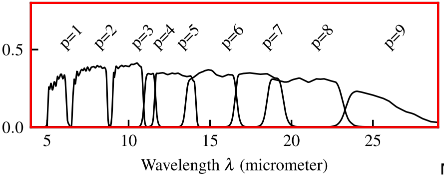

spectral bands of the MIRI Imager

Complete Equation of the Model

For p-th spectral band and (i,j)-th pixel :

$$y_{i,j}^{(p)} = \int_{\mathbb{R}_+} \omega_p(\lambda) \left(\iint_{\Omega_{\text{pix}}} \underbrace{\left(\iint_{\mathbb{R}^2} \phi(\alpha', \beta', \lambda) h(\alpha - \alpha', \beta - \beta', \lambda) d\alpha' d\beta' \right)}_{\textbf{2D Convolution with the variant PSF}} b_{\text{samp}}(\alpha - \alpha_i, \beta - \beta_j) d\alpha d\beta \right) d\lambda + n_{i,j}^{(p)}$$

where $p = 1, \ldots, P, i = 1, \ldots, N_i, j = 1, \ldots, N_j$

- N_i and N_j are numbers of rows and columns of the detector matrix
- P is the number of bands
- h is the PSF (Point Spread Function).
- ω_p is the spectral response of the instrument (filter + detector).
- b_{samp} is a spatial sampling function over the pixel area Ω_{pix} and $n_{i,j}^{(p)}$ is an additive noise.

Hypothesis : The non-ideal characteristics of the detector are assumed to be corrected upstream.

Illustration of the Object Model

Spectral distribution at k, l-th pixel with $P = 5$ spectral bands

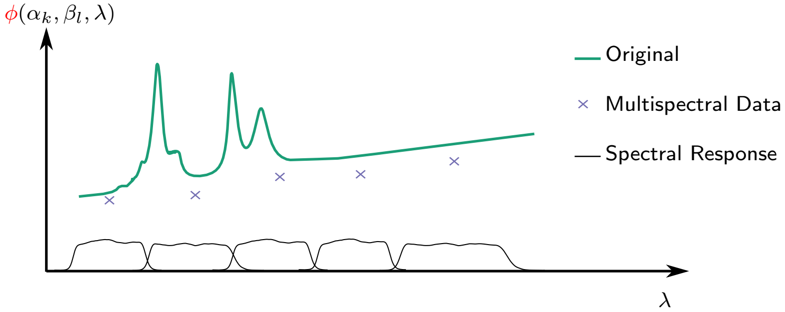

Representation with a piecewise linear function :

$$\phi(\alpha, \beta, \lambda) = \sum_{m=1}^{N_\lambda} \sum_{k=1}^{N_k} \sum_{l=1}^{N_l} x_{k,l}^{(m)} \, b_{\text{spat}}(\alpha - \alpha_k, \beta - \beta_l) b_{\text{spec}}(\lambda)$$

b_{spat} is a uniform discretization function and b_{spec} a first-order B-spline. N_λ number of wavelengths

Illustration of the Object Model

Spectral distribution at k, l-th pixel with $P = 5$ spectral bands

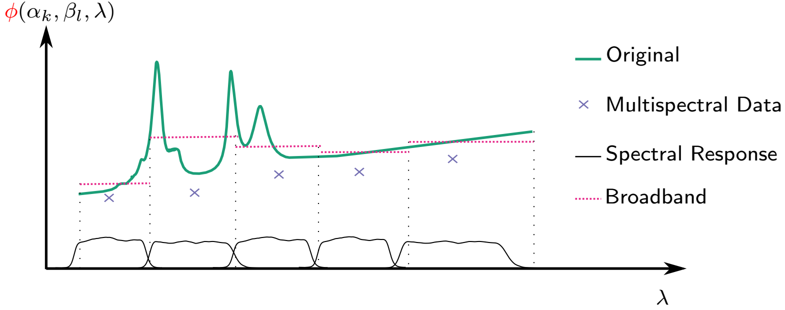

Representation with a piecewise linear function :

$$\phi(\alpha, \beta, \lambda) = \sum_{m=1}^{N_\lambda} \sum_{k=1}^{N_k} \sum_{l=1}^{N_l} x_{k,l}^{(m)} \, b_{\text{spat}}(\alpha - \alpha_k, \beta - \beta_l) b_{\text{spec}}(\lambda)$$

b_{spat} is a uniform discretization function and b_{spec} a first-order B-spline. N_λ number of wavelengths

Illustration of the Object Model

Spectral distribution at k, l-th pixel with $P = 5$ spectral bands

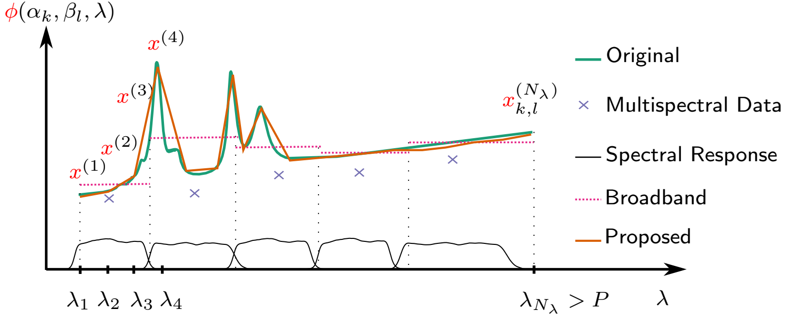

Representation with a piecewise linear function :

$$\phi(\alpha, \beta, \lambda) = \sum_{m=1}^{N_\lambda} \sum_{k=1}^{N_k} \sum_{l=1}^{N_l} x_{k,l}^{(m)} \, b_{\text{spat}}(\alpha - \alpha_k, \beta - \beta_l) b_{\text{spec}}(\lambda)$$

b_{spat} is a uniform discretization function and b_{spec} a first-order B-spline. N_λ number of wavelengths

Forward Model

By substituting the object model in the instrument model we obtain :

$$\boldsymbol{y}^{(p)} = \sum_{m=1}^{N_\lambda} \boldsymbol{H}^{p,m} \boldsymbol{x}^{(m)} + \boldsymbol{n}^{(p)}, \quad p = 1, \ldots, P$$

$$H^{p,m}_{i,j;k,l} = \iint_{\Omega_{\text{pix}}} \left(\left(\int_{\mathbb{R}_+} \omega_p(\lambda) h(\alpha, \beta, \lambda) b_{\text{spec}}(\lambda) d\lambda \right) \underset{\alpha,\beta}{*} b_{\text{spat}}(\alpha - \alpha_k, \beta - \beta_l) \right) b_{\text{samp}}(\alpha - \alpha_i, \beta - \beta_j) d\alpha d\beta$$

By joint processing of all multispectral data : Multichannel processing

$$\underbrace{\begin{pmatrix} \boldsymbol{y}^{(1)} \\ \boldsymbol{y}^{(2)} \\ \vdots \\ \boldsymbol{y}^{(P)} \end{pmatrix}}_{\boldsymbol{y}} = \underbrace{\begin{pmatrix} \boldsymbol{H}^{1,1} & \boldsymbol{H}^{1,2} & \cdots & \boldsymbol{H}^{1,N_\lambda} \\ \boldsymbol{H}^{2,1} & \boldsymbol{H}^{2,2} & \cdots & \boldsymbol{H}^{2,N_\lambda} \\ \vdots & \vdots & \ddots & \vdots \\ \boldsymbol{H}^{P,1} & \boldsymbol{H}^{P,2} & \cdots & \boldsymbol{H}^{P,N_\lambda} \end{pmatrix}}_{\boldsymbol{H}} \underbrace{\begin{pmatrix} \boldsymbol{x}^{(1)} \\ \boldsymbol{x}^{(2)} \\ \vdots \\ \boldsymbol{x}^{(N_\lambda)} \end{pmatrix}}_{\boldsymbol{x}} + \underbrace{\begin{pmatrix} \boldsymbol{n}^{(1)} \\ \boldsymbol{n}^{(2)} \\ \vdots \\ \boldsymbol{n}^{(P)} \end{pmatrix}}_{\boldsymbol{n}}$$

$$\boldsymbol{y} = \boldsymbol{H}\boldsymbol{x} + \boldsymbol{n}$$

Regularized Least-Squares

Convex Minimization :

$$\hat{\boldsymbol{x}} = \underset{\boldsymbol{x}}{\text{argmin}} \ \mathcal{J}(\boldsymbol{x})$$

where the objective function is

$$\mathcal{J}(\boldsymbol{x}) = \underbrace{\|\boldsymbol{y} - \boldsymbol{H}\boldsymbol{x}\|_2^2}_{\substack{\mathcal{Q}(\boldsymbol{x},\boldsymbol{y}) \\ \text{Data fidelity}}} + \underbrace{\left\{ \mu_{\text{spat}} \underbrace{\|\boldsymbol{D}_{\text{spat}}\boldsymbol{x}\|_2^2}_{\mathcal{R}_{\text{spat}}(\boldsymbol{x})} + \mu_{\text{spec}} \underbrace{\|\boldsymbol{D}_{\text{spec}}\boldsymbol{x}\|_2^2}_{\mathcal{R}_{\text{spec}}(\boldsymbol{x})} \right\}}_{\text{Quadratic Regularizations}}$$

$\boldsymbol{D}_{\text{spat}}$ and $\boldsymbol{D}_{\text{spec}}$ are 2D and 1D finite difference operator along the spatial and spectral dimensions to enforce smoothness. μ_{spat} and μ_{spec} are regularization parameters.

Solution of the Problem : $\mathcal{J}$ is linear and differentiable

$$\hat{\boldsymbol{x}} = \left(\boldsymbol{H}^T\boldsymbol{H} + \mu_{\text{spat}}\boldsymbol{D}_{\text{spat}}^T\boldsymbol{D}_{\text{spat}} + \mu_{\text{spec}}\boldsymbol{D}_{\text{spec}}^T\boldsymbol{D}_{\text{spec}}\right)^{-1}\boldsymbol{H}^T\boldsymbol{y}.$$

Computation of the Solution

Computation of the solution requires the inversion of the Hessian matrix :

$$\boldsymbol{Q}^{-1} = \left(\boldsymbol{H}^T\boldsymbol{H} + \mu_{\text{spat}}\boldsymbol{D}_{\text{spat}}^T\boldsymbol{D}_{\text{spat}} + \mu_{\text{spec}}\boldsymbol{D}_{\text{spec}}^T\boldsymbol{D}_{\text{spec}}\right)^{-1}$$

Computation limit ! $\boldsymbol{Q} \in \mathbb{R}^{N_\lambda N_k N_l \times N_\lambda N_k N_l}$ is a high-dimensional block-matrix, e.g. 3932160×3932160 $(N_k = N_l = 256, N_\lambda = 60)$
$\rightarrow$ heavy to inverse and requires a very large memory.

Proposition :

Computation of the solution iteratively without matrix inversion using an optimization algorithm such as the **Conjugated gradient algorithm**.

$$\boldsymbol{Q}\boldsymbol{x} = \boldsymbol{H}^T\boldsymbol{y}$$

Setup of the Experiment

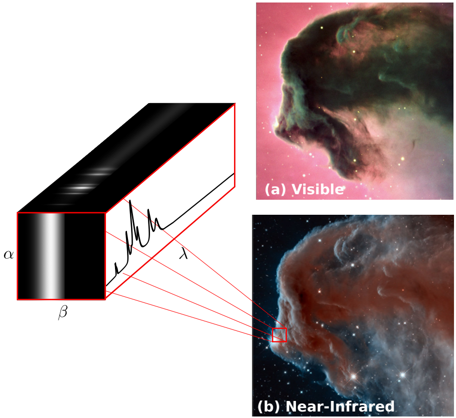

- Size of the original object $\mathbf{1024 \times 256 \times 256}$

Simulation Results

Multispectral data of the JWST/MIRI Imager

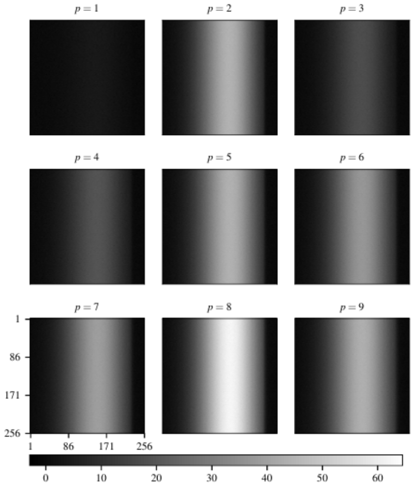

- Size of the multispectral data $\mathbf{9 \times 256 \times 256}$

- Additive white Gaussian noise (σ_n) of $\mathbf{SNR{=}30\ dB}$

$$\mathrm{SNR} = 10\log_{10}\left(\frac{\frac{1}{N}\|\boldsymbol{y}\|_2^2}{\sigma_n^2}\right)$$

Reconstruction Results

Spatial distribution at $\lambda = 7.8, 16, 21$ μm with $N_\lambda = 60$

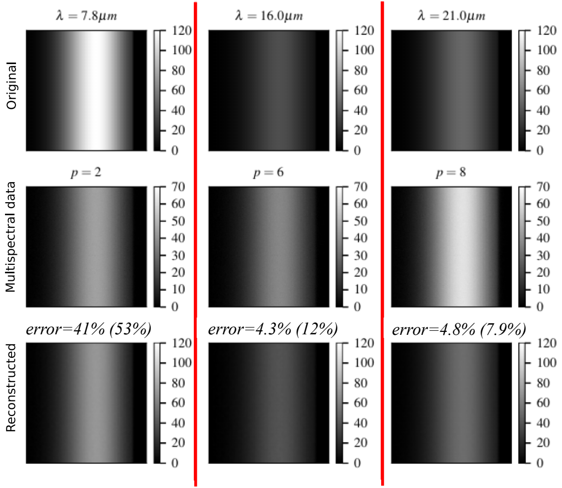

- Reconstruction error :

$$\text{Error} = \frac{\|\boldsymbol{x}_{orig} - \boldsymbol{x}_{rec}\|_2}{\|\boldsymbol{x}_{orig}\|_2}$$

Reconstruction Results

Spectral Distribution at pixel $(127, 100)$

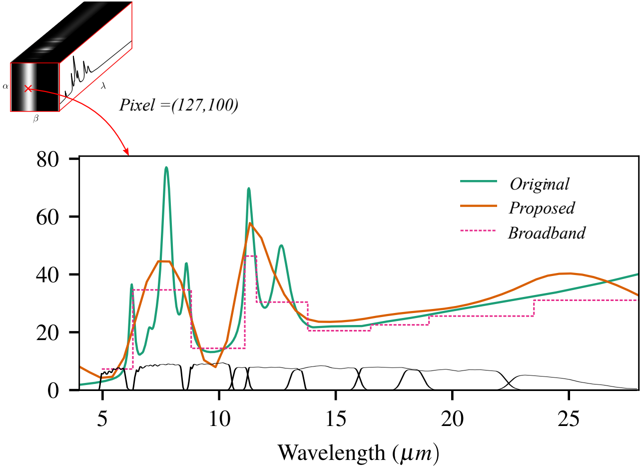

Conclusion

- Better object reconstruction compared to conventional approaches (Improvement factor up to $\mathbf{2.6}$).
- Modeling the response of the JWST/MIRI Imager by accounting for a spectral-variant PSF, detector sampling and integration.
- Representing the object spectral distribution with a first-order B-spline
- Joint processing of the multispectral data from different bands
- Multichannel reconstruction using regularization approach

Perspectives

- Compute the solution in the Fourier space for faster computation
- Propose a solution for tuning N_λ and the regularization parameters
- Explore other object representation (e.g. linear mixing model)

Thank You
for
Your Attention.

References I

[Abergel *et al.* 2003] A Abergel, D Teyssier, JP Bernard, F Boulanger, A Coulais, D Fosse, E Falgarone, M Gerin, M Perault, J-L Puget*et al.*

ISOCAM and molecular observations of the edge of the Horsehead nebula.

Astronomy & Astrophysics, vol. 410, no. 2, pages 577–585, 2003.

[Aniano *et al.* 2011] G Aniano, BT Draine, KD Gordon and K Sandstrom.

Common-resolution convolution kernels for space-and ground-based telescopes.

Publications of the Astronomical Society of the Pacific, vol. 123, no. 908, page 1218, 2011.

[Bouchet *et al.* 2015] Patrice Bouchet, Macarena García-Marín, P-O Lagage, Jérome Amiaux, J-L Auguéres, Eva Bauwens, JADL Blommaert, CH Chen, ÖH Detre, Dan Dicken*et al.*

The Mid-Infrared Instrument for the James Webb Space Telescope, III : MIRIM, The MIRI Imager.

Publications of the Astronomical Society of the Pacific, vol. 127, no. 953, page 612, 2015.

[Geis & Lutz 2010] N Geis and D Lutz.

Herschel/PACS modelled point-spread functions, 2010.

[Guillard *et al.* 2010] Pierre Guillard, Thomas Rodet, S Ronayette, J Amiaux, Alain Abergel, V Moreau, JL Augueres, A Bensalem, T Orduna, C Nehmé*et al.*

Optical performance of the JWST/MIRI flight model : characterization of the point spread function at high resolution.

In SPIE Astronomical Telescopes+ Instrumentation, pages 77310J–77310J. International Society for Optics and Photonics, 2010.

References II

[Hadj-Youcef *et al.* 2017] MA Hadj-Youcef, François Orieux, Aurélia Fraysse and Alain Abergel.

Restoration from multispectral blurred data with non-stationary instrument response.

In Signal Processing Conference (EUSIPCO), 2017 25th European, pages 503–507. IEEE, 2017.

[Perrin *et al.* 2014] Marshall D Perrin, Anand Sivaramakrishnan, Charles-Philippe Lajoie, Erin Elliott, Laurent Pueyo, Swara Ravindranath and Loïc Albert.

Updated point spread function simulations for JWST with WebbPSF.

In Space Telescopes and Instrumentation 2014 : Optical, Infrared, and Millimeter Wave, volume 9143, page 91433X. International Society for Optics and Photonics, 2014.

[Soulez *et al.* 2013] Ferréol Soulez, Eric Thiébaut and Loıc Denis.

Restoration of hyperspectral astronomical data with spectrally varying blur.

EAS Publications Series, vol. 59, pages 403–416, 2013.

[Villeneuve & Carfantan 2014] E. Villeneuve and H. Carfantan.

Nonlinear Deconvolution of Hyperspectral Data With MCMC for Studying the Kinematics of Galaxies.

IEEE Transactions on Image Processing, vol. 23, no. 10, pages 4322–4335, Oct 2014.